

PhysGNN: A Physics–Driven Graph Neural Network Based Model for Predicting Soft Tissue Deformation in Image–Guided Neurosurgery

Yasmin Salehi, Dennis Giannacopoulos

Department of Electrical and Computer Engineering, McGill University, Canada
 yasmin.salehi@mail.mcgill.ca,
 dennis.giannacopoulos@mcgill.ca.

Abstract

Correctly capturing intraoperative brain shift in image-guided neurosurgical procedures is a critical task for aligning preoperative data with intraoperative geometry, ensuring effective surgical navigation and optimal surgical precision. While the finite element method (FEM) is a proven technique to effectively approximate soft tissue deformation through biomechanical formulations, their degree of success boils down to a trade-off between accuracy and speed. To circumvent this problem, the most recent works in this domain have proposed leveraging data-driven models obtained by training various machine learning algorithms—e.g. random forests, artificial neural networks (ANNs)—with the results of finite element analysis (FEA) to speed up tissue deformation approximations by prediction. These methods, however, do not account for the structure of the finite element (FE) mesh during training that provides information on node connectivities as well as the distance between them, which can aid with approximating tissue deformation based on the proximity of force load points with the rest of the mesh nodes. Therefore, this work proposes a novel framework, PhysGNN, a data-driven model that approximates the solution of FEA by leveraging graph neural networks (GNNs), which are capable of accounting for the mesh structural information and inductive learning over unstructured grids and complex topological structures. Empirically, we demonstrate that the proposed architecture, PhysGNN, promises accurate and fast soft tissue deformation approximations while remaining computationally feasible, suitable for neurosurgical settings.

Introduction

Exploiting high-quality preoperative images for surgical planning is a common practice among neurosurgeons. With the recent advances in surgical tools, medical imagery techniques have especially made their way into operating rooms to enhance surgical visualization and navigation, giving rise to image-guided neurosurgical techniques, where correctly aligning patient’s intraoperative anatomical geometry with preoperative images has a significant impact on the accuracy of surgical navigation [Hagemann et al. 1999, Warfield et al. 2000, Ferrant et al. 2002, Sun et al. 2004, Vigneron et al. 2004, Choi et al. 2004, Miller et al. 2007, Wittek et al. 2009, Joldes et al. 2009, Vigneron et al. 2010, Wittek et al. 2010, Li et al. 2014, Miller et al. 2019]. This task, however, poses

a challenge. During the neurosurgical procedure, the brain continuously undergoes a series of anatomical changes for a variety of reasons such as gravity, craniotomy¹, tissue retraction and resection, and anesthetics [Roberts et al. 1998], making surgical navigation based on preoperative data alone error-prone and unreliable [Wittekk et al. 2010].

To account for intraoperative brain shift², registration technology, by which the coordinate system of preoperative data and surgical site are brought into spatial alignment, has emerged as an essential tool in image-guided surgical frameworks for maintaining surgical navigation accuracy and depth perception [Crum et al. 2004, Cleary and Peters 2010, Risholm et al. 2011]. In a registration framework, data alignment is achieved by leveraging interpolation and transformation functions, which manipulate preoperative data to realize tissue deformations and are regularized by a constraint [Ferrant et al. 2002].

At large, registration approaches may be categorized into image-based and model-based methods, which differ in the type of prior information they use as a constraint for deforming preoperative data with respect to intraoperative geometry. To define, image-based registration methods are a set of techniques which mainly use pixel/voxel information and solely rely on image processing techniques to realize tissue deformation [Beauchemin and Barron 1995, Hata et al. 2000, Ji et al. 2014, Iversen et al. 2018, Tu et al. 2019]. While they may be effective in some settings—e.g. registering deformations of hard tissues such as bone—they are prone to failing in effectively capturing *soft* tissue deformation for various reasons, such as contrast variations between preoperative and intraoperative images resulted from use of different image acquisition techniques, disappearance of boundaries between tissues upon surgical cuts, and presence of contrast agents [Ferrant et al. 2002]. But most importantly, image-based techniques neglect prior information about the biomechanical behaviour of soft tissue, which is an essential knowledge for creating accurate volumetric mappings [Nabavi et al. 2001, Ferrant et al. 2002].

On the other hand, model-based methods are a set of

¹Temporarily removing part of the bone from skull to access the brain tissue.

²Volumetric brain deformations induced by surgical operations [Nabavi et al. 2001].

registration techniques that treat images as *deformable volumes*—a notion first introduced by Broit [1981]—to better allow for presenting elastic and plastic deformations. These approaches address intraoperative registration challenges by imposing additional constraints—based on mathematical or physical characterization of soft tissue [Zhang et al. 2017]—to compute soft tissue deformation, resulting in mathematical- and physics-based solution formulations. In particular, studying physics-based methods has become an emerging area of research in recent years [Choi et al. 2004, Joldes et al. 2009, Malone et al. 2010, Wittek et al. 2010, Joldes et al. 2010, Basafa and Farahmand 2011, Miller et al. 2019] for their potential to accurately model the biomechanics of the brain and *predicting* soft tissue deformation. Indeed, recent advances in this domain have led to the innovation of advanced image-guided surgical systems that are equipped with augmented reality (AR), which is established by fusing virtual reality (VR) with high-quality preoperative images in the form of a deformable volume [Cleary and Peters 2010]. The goal of integrating AR in this framework is to facilitate tracking predefined surgical access routes without having to look away from the screen, and provide surgeons with visual tool-tissue interaction [Tonutti et al. 2017].

In the literature, the finite element method (FEM) is a powerful technique for generating 3-dimensional (3D) deformable volumes from high-quality preoperative images, which can simulate intraoperative brain deformations [Wittek et al. 2010]. However, their degree of success boils down to a trade-off between accuracy and speed [Tonutti et al. 2017]. In most cases, benefiting from a finite element (FE) model, which accounts for all types of material and geometric non-linearities, is not always feasible for requiring significant computational resources [Wittek et al. 2010, Tonutti et al. 2017]. To address this limitation, recent works have proposed deriving deformable models by training machine learning algorithms with the results of precomputed FEM simulations that are based on preoperative images [De et al. 2011, Tonutti et al. 2017, Lorente et al. 2017, Pfeiffer et al. 2019, Liu et al. 2020]. However, while promising, they all lack a key aspect for effectively learning over mesh data: they do not account for graph structure—e.g. node connectivities—which is an important piece of information for learning nodal displacements within each finite element resulted from prescribed loads. In fact, wanting to incorporate node connectivities by feeding the adjacency matrix as a set of features to the aforementioned algorithms will result in an ill-posed problem as the number of features would then exceed the number of data points. Additionally, these methods are arguably computationally inefficient and hard to train for high quality meshes—which contain many nodes—as the number of parameters needed to train the models would be in order of $O(|\mathcal{V}|)$, where $|\mathcal{V}|$ is the number of mesh nodes. Although the later problem has been previously addressed by training only on a subset of the mesh data [Tonutti et al. 2017], or capturing a lower dimensional embedding of the deformation space through Principle Component Analysis (PCA) [Liu et al. 2020], an important question is raised on whether we can enhance computational feasibility while also benefiting from the structural information of

the finite element mesh.

Present Work. In this work, we propose a novel data-driven framework, named PhysGNN³, which is based on two types of Graph Neural Networks (GNNs) [Scarselli et al. 2008], namely GraphSAGE- [Hamilton et al. 2017a] and Graph-Conv [Morris et al. 2019], that is trained with the results of Finite Element Analysis (FEA), and thus is based on the physical characteristics of soft tissue. The motivation behind using GNNs for capturing tissue deformation upon prescribed loads is their ability to define deep neural networks on graph data. Specifically, GNNs are a class of node embedding techniques⁴ that enable generalization of convolution on graph data through the notion of *neural message passing* [Gilmer et al. 2017], by which the information of nodes within a neighbourhood of an arbitrary size are transformed and aggregated producing a new value [Hamilton 2020]. The message passing framework enables inductive learning over graphs through *parameter sharing*, a property that ensures learning a constant number of parameters independent of the mesh size. Therefore, contrary to the previous methods, not only is PhysGNN capable of incorporating mesh structural information—i.e. proximity of mesh nodes with each other and the Euclidean distance of neighbouring nodes from one another—which can aid with effective prediction of tissue deformation, but also enhances computational feasibility when learning from high quality meshes that consist of many nodes.

We evaluate the performance of PhysGNN on two datasets, which are distinguished by the number of force load points and the total force applied. Through our empirical results, we demonstrate that PhysGNN is capable of successfully predicting tissue deformation upon prescribed forces under 0.005 and 1.9 seconds using a GPU and CPU, respectively. In fact, the absolute displacement error of PhysGNN for 97% of the nodes is found to be under 1 mm—which is the precision in neurosurgery [Miller et al. 2010].

Related Work

Approximating Tissue Deformation with Machine Learning. The predictive power of various machine learning algorithms in approximating tissue deformation with respect to physics laws has been assessed in a number of studies. These approaches either implement machine learning techniques as an alternative to the FEM—e.g. representing mass points as cellular neural networks to assimilate elastic deformations [Zhong et al. 2006, Zhang et al. 2019]—or as a subsequent step to preoperative FEA in which data-driven models are resulted by training machine learning models with patient-generated data to predict soft tissue deformation, as shown in Figure 1. For example, while De et al. [2011] proposed a physics-driven framework, named PhyNNeSS, consisting of radial basis

³The data and implementation will be made available at <https://github.com/TBA>

⁴Node embedding techniques are a set of approaches that encode graph data—e.g. nodes, edges, features—into a lower dimensional vector space [Hamilton et al. 2017b].

function to reconstruct the deformation fields of liver and Penrose drain models, Lorente et al. [2017] investigated the success of linear regression, decision trees, random forests, and extremely randomized trees in simulating the biomechanical behavior of human liver under large deformations and during breathing in real time. Furthermore, Liu et al. [2020] exploited ANNs to reconstruct tissue deformation of a head and neck tumour, where the dataset was encoded into a low-dimensional representation using PCA prior to training to facilitate the learning process.

Meanwhile, similar techniques have been employed to approximate brain deformation in neurosurgical settings. In [Tonutti et al. 2017], the authors explore and compare the effectiveness of ANNs and support vector regression (SVR) in predicting a brain tumour tissue deformation caused by applying forces to the brain tissue. Generalizing the notion of deep learning based soft tissue simulation frameworks to different types of organs, Pfeiffer et al. [2019] proposed a convolutional neural network (CNN) based soft tissue simulation system to predict an organ’s internal deformation from known surface deformation. In their study, they account for *all* tissue types within an organ and train the CNNs on an entirely synthetic data of random organ-like meshes to enhance the learning process by using more data than otherwise available. They state their method can be adopted by the neurosurgical community to capture brain shift or be used in motion compensation radiotherapy.

Learning Mesh-Based Simulations Using GNNs. Belbute-Peres et al. [2020] have previously proposed a Graph Convolution Network (GCN) [Kipf and Welling 2016] based architecture to learn fluid flow prediction. More recently, Sanchez-Gonzalez et al. [2020] and Pfaff et al. [2020] have proposed Graph Network-based Simulators (GNS) and MeshGraphNets respectively—both GraphNet [Sanchez-Gonzalez et al. 2018] based generative architectures—to simulate interaction of fluids, rigid solids, and deformable materials with one another [Sanchez-Gonzalez et al. 2020], and complex physical systems such as aerodynamics, structural mechanics, and cloth [Pfaff et al. 2020].

The Physics-Driven Graph Neural Network (PhysGNN) Model

PhysGNN is a data-driven model that leverages GNNs to learn the nonlinear behavior of soft tissue under prescribed loads from FE simulations. In this work, GNNs are deemed as the most suitable deep learning candidates for capturing tissue deformation for two reasons.

1. First, GNNs enable incorporating mesh structural information by forming a computation graph—a neural network architecture—for every node through unfolding the neighbourhood around them via neural message passing, which refers to the exchange of feature and structural information between nodes that are within the same k -hop neighbourhood [Hamilton 2020]. This characteristic of GNNs can ensure more accurate prediction of tissue deformation that is especially in close proximity of prescribed forces and susceptible to undergoing larger displacements, since the distance between prescribed force

nodes and free-boundary condition nodes can be accounted for.

2. Second, GNNs learn the same weight and bias parameters across the FE mesh through parameter sharing. In other words, the number of parameters which need to be learned are constant and independent of the mesh size, a property that also enables generalization of GNNs to unseen parts of the graph. This makes training PhysGNN with high quality meshes—which inherently consist of many nodes—computationally less expensive than the methods presented in the previous studies.

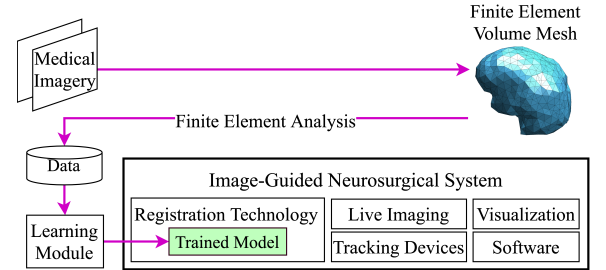


Figure 1: A generic image-guided neurosurgical system framework [Cleary and Peters 2010], where patient’s anatomy is aligned with preoperative images through deforming a deformable volume generated from preoperative imagery, which its biomechanical behavior under prescribed loads is predicted by machine learning methods.

Architecture

To capture tissue deformation, PhysGNN incorporates two types of GNNs, namely GraphSAGE [Hamilton et al. 2017a] and GraphConv, which is the graph convolution operator of k -GNNs in [Morris et al. 2019]. The message passing architecture of GraphSAGE and GraphConv for a graph $\mathcal{G} = (\mathcal{V}, \mathcal{E})$, with \mathcal{V} and \mathcal{E} being the vertex and edge sets respectively, $u, v \in \mathcal{V}$, and matrix $\mathbf{X} \in \mathbb{R}^{d \times |\mathcal{V}|}$ representing the node features, are defined as:

$$\mathbf{m}_{\mathcal{N}(u)}^{(k)} = \text{AGGREGATE}^{(k)}(\{\mathbf{h}_v^{(k-1)}, \forall v \in \mathcal{N}(u)\})$$

$$\mathbf{h}_u^{(k)} = [\mathbf{W}_{\text{self}}^{(k)} \cdot \mathbf{h}_u^{(k-1)} \oplus \mathbf{W}_{\text{neigh}}^{(k)} \cdot \mathbf{m}_{\mathcal{N}(u)}^{(k)} + \mathbf{b}^{(k)}], \quad (1)$$

and

$$\mathbf{m}_{\mathcal{N}(u)}^{(k)} = \text{AGGREGATE}^{(k)}(\{e_{vu} \cdot \mathbf{h}_v^{(k-1)}, \forall v \in \mathcal{N}(u)\})$$

$$\mathbf{h}_u^{(k)} = \text{UPDATE}^{(k)}[\mathbf{W}_{\text{self}}^{(k)} \cdot \mathbf{h}_u^{(k-1)},$$

$$\mathbf{W}_{\text{neigh}}^{(k)} \cdot \mathbf{m}_{\mathcal{N}(u)}^{(k)} + \mathbf{b}^{(k)}], \quad (2)$$

respectively, where $\mathcal{N}(u)$ is the neighbourhood of node u , $\mathbf{m}_{\mathcal{N}(u)}^{(k)}$ represents the aggregated messages from the neighbours of node u at iteration k , where $k \in \{1, \dots, K\}$, \mathbf{h}_u and \mathbf{h}_v are the embedding for nodes u and v respectively, e_{uv} is the edge weight between node u and v , \oplus is the concatenation operator, AGGREGATE and UPDATE are arbitrary differentiable functions, and the weights, $\mathbf{W}_{\text{self}}^{(k)}, \mathbf{W}_{\text{neigh}}^{(k)} \in$

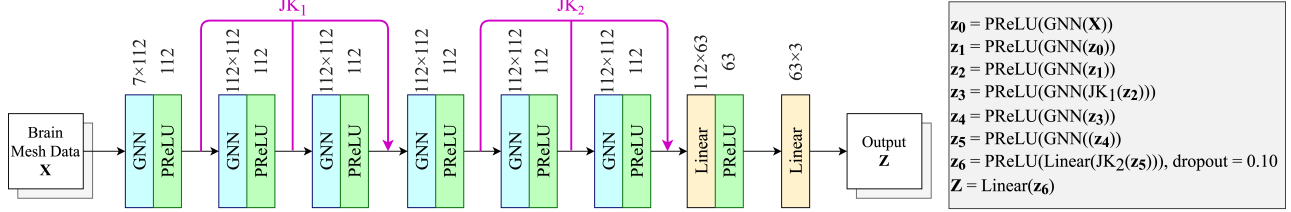


Figure 2: Architectural Diagram of PhysGNN.

$\mathbb{R}^{d^k \times d^{(k-1)}}$, and the bias term, $\mathbf{b}^{(k)} \in \mathbb{R}^{d^{(k)}}$, are trainable parameters. Moreover, the input to the GNN is simply the node features, expressed as $\mathbf{h}_u^0 = \mathbf{x}_u, \forall u \in \mathcal{V}$, while the output of the final layer for each node is $\mathbf{z}_u = \mathbf{h}_u^K, \forall u \in \mathcal{V}$.

In this work, K is set to 6—i.e. the mesh nodes capture information from their 6-hop neighborhood. Additionally, the implemented AGGREGATE functions are maximum and summation, while the UPDATE function used for the GraphConv layers is concatenation. PhysGNN also benefits from a variation of jumping knowledge (JK) connections [Xu et al. 2018] to combat over-smoothing, which generates a weighted sum of embeddings at different iterations by long short-term memory (LSTM) attention layers as:

$$\sum_{t=1}^T \alpha_u^{(t)} \mathbf{h}_u^{(t)}, \quad (3)$$

where $\alpha_u^{(t)}$ are the attention scores. A full architectural diagram of PhysGNN is illustrated in Figure 2.

It should be noted that different variations of PhysGNN can be obtained by changing the combination of GraphConv and GraphSAGE layers, as well as the aggregation function they use. The performance of various configurations of PhysGNN on two different datasets is presented in the Results and Discussion section.

Experimental Setting

Data Acquisition

Generating the Finite Element Mesh. The FE volume mesh for running FE simulations was generated by running TetGen [Si 2015] on the surface mesh files provided by Tonutti et al. [2017], which is based on MRI scans taken from the Repository of Molecular Brain Neoplasia Data [Madhavan et al. 2009]. Figure 3a is illustrative of the FE volume mesh and Table 1 details over the characteristics of it.

Material Properties. Based on the work done in [Joldes et al. 2010] and [Wittek et al. 2010], the mechanical behavior of healthy brain and tumour tissues were characterized as hyper-elastic material obeying the Neo-Hookean constitutive law:

$$W = \frac{2\mu}{\alpha^2} (\lambda_1^\alpha + \lambda_2^\alpha + \lambda_3^\alpha - 3), \quad (4)$$

where W is the energy, μ is the shear modulus in undeformed state, α is a material coefficient, and λ is the principal longitudinal stretch. In this experimental setting, the

Attribute	Value
Mesh points	9118
Mesh tetrahedra	55927
Mesh faces	112524
Mesh faces on exterior boundary	1340
Mesh faces on input facets	2992
Mesh edges on input segments	4488
Steiner points inside domain	7618

Table 1: Volume Mesh Statistics.

tumour and healthy brain tissues have identical density and Poisson ratio. However, the tumour was assumed to be stiffer than the healthy brain tissue, thus having a larger Young’s modulus. The numerical value of material parameters can be found in Table 2.

Dataset	Density (kg/m ³)	Young’s Modulus (Pa)	Poisson Ratio
Healthy Tissue	1000	3000	0.49
Tumour	1000	7500	0.49

Table 2: Material properties of different parts of the brain [Joldes et al. 2010, Wittek et al. 2010].

FE Simulations. To assess the effectiveness of PhysGNN in predicting tissue deformation imposed by forces, two different datasets were generated by running FE simulations on the FE mesh in FEBio [Maas et al. 2012] using the GIBBON [Moerman 2018] toolbox. The datasets are distinguished by the total force applied and the number of prescribed load nodes. Specifically, Dataset 1 was acquired by applying 1.35N to 1 node at a time in 30 different time steps and 15 directions for a total of 11 different nodes. This choice was motivated by the results of the experimental study done by Gan et al. [2015] who measured 70% of induced forces during neurosurgery to be less than 0.3N and a maximal peak at 1.35N during craniotomy. On the other hand, Dataset 2 was created by applying 20N to 100 nodes at a time in 30 different time steps and 165 directions to further capture the non-linear behavior of soft tissue under large forces. Therefore, the amount of force applied to each prescribed node in Dataset 1 at time i is:

$$\mathbf{F}_i = \frac{\mathbf{F}_{\text{total}}}{30} \times i, \quad i \in \{1, \dots, 30\}, \quad (5)$$

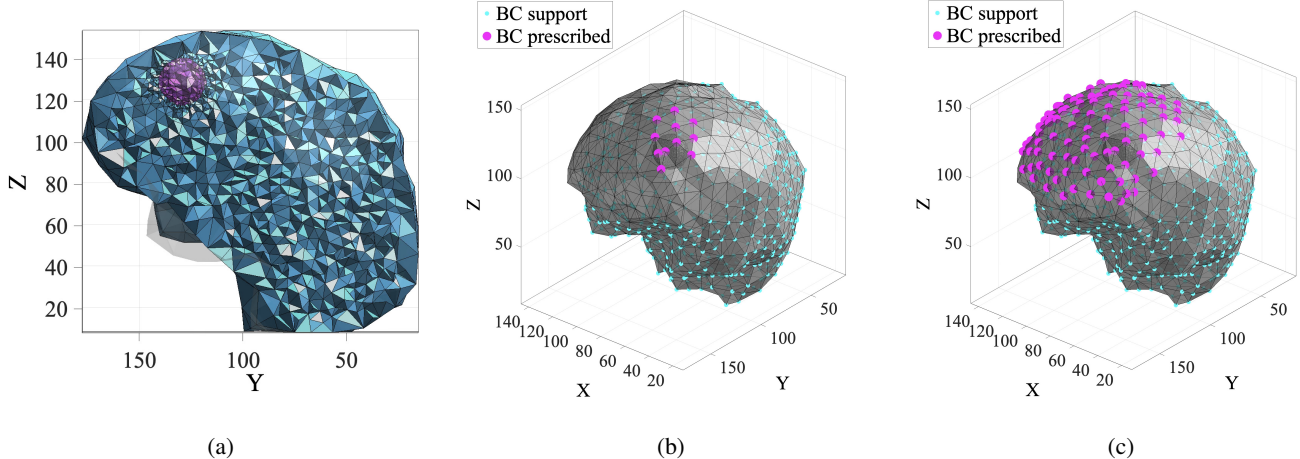


Figure 3: (a) Cut view of the FE volume mesh, where cyan represents the healthy brain tissue, while magenta represents the tumour tissue; (b) prescribed and fixed boundary condition nodes of Dataset 1; (c) prescribed and fixed boundary condition nodes of Dataset 2.

Dataset	No. Fixed B.C. Nodes	No. Pres. Load Nodes	No. Pres. Load Node(s) / Simulation	No. Force Magnitudes	Max. Force Applied (N)	No. Directions	No. Simulations
1	502	11	1	30	1.35	15	4950
2	502	100	100	30	20	165	4950

Table 3: Generated datasets information. B.C. stands for Boundary Condition. Pres. stands for Prescribed.

whereas the amount of force applied to one of the prescribed nodes in Dataset 2 at time i is:

$$\mathbf{F}_i = \frac{\mathbf{F}_{\text{total}}}{30 \times 100} \times i, \quad i \in \{1, \dots, 30\}. \quad (6)$$

The direction of forces applied to each prescribe load node features its surface normal direction, as well as directions that are randomly sampled from a hemisphere with radius 1. Lastly, to train PhysGNN, a train:validation:test split of 70:20:10 was applied to both datasets. Figures 3b and 3c are illustrative of the prescribed load nodes in Datasets 1 and 2 respectively, which are located near the tumour site, as well as the fixed boundary condition nodes, which mimic the skull bone that prevents tissue from moving. Further details on the generated datasets can be found in Table 3.

Features (X)	Output (Z)
$F_x, F_y, F_z, F_\rho, F_\theta, F_\phi$, Physical Property	$\delta x, \delta y, \delta z$

Table 4: PhysGNN features and outputs.

Features and Output

The features inputted into PhysGNN, summarized in Table 4, are the force value applied to prescribed load nodes in Cartesian and polar coordinates, denoted as (F_x, F_y, F_z) and $(F_\rho, F_\theta, F_\phi)$ as well as a constant value, named Physical

Property, which is set to:

$$\begin{cases} 0.4, & \text{if the node belongs to tumour tissue, and} \\ 1, & \text{if the node belongs to healthy brain tissue,} \end{cases}$$

for nodes with free boundary condition, and 0 if otherwise. This value determines how much a node can undergo displacements based on its boundary condition and Young's Modulus considering that brain tissue is susceptible to undergoing larger displacements for its smaller Young's Modulus compared to the tumour tissue. In particular, the value of 0.4 was calculated as:

$$\frac{\text{Young's Modulus}_{\text{healthy tissue}}}{\text{Young's Modulus}_{\text{tumour tissue}}} = \frac{3000}{7500} = 0.4.$$

Lastly, for the GraphConv models, the edge weights were calculated as the inverse of the Euclidean distance between adjacent nodes u and v with $u, v \in \mathcal{V}$ as:

$$e_{u,v} = \frac{1}{\sqrt{((x_u - x_v)^2 + (y_u - y_v)^2 + (z_u - z_v)^2)}}. \quad (7)$$

Loss Function and Optimization

The loss function used for learning the trainable parameters is the mean Euclidean error computed as:

$$\mathcal{L} = \frac{1}{|\mathcal{V}|} \sum_{v \in \mathcal{V}} \sqrt{\sum_{i=1}^3 (\mathbf{y}_{v,i} - \mathbf{z}_{v,i})^2}, \quad (8)$$

Dataset	MAE (δx) (mm)	MAE (δy) (mm)	MAE (δz) (mm)	Mean Euclidean Error (mm)	% Euclidean Error $\leq 1\text{mm}$	Mean Absolute Position Error (mm)	% Absolute Position Error $\leq 1\text{mm}$
Dataset 1 Validation	0.1145 \pm 0.2832	0.1051 \pm 0.2544	0.1009 \pm 0.2650	0.2105 \pm 0.4530	94.99	0.1690 \pm 0.4200	95.91
	0.1117 \pm 0.2750	0.0999 \pm 0.2318	0.0999 \pm 0.2601	0.2049 \pm 0.4329		0.1612 \pm 0.3961	96.18
Dataset 2 Validation	0.1478 \pm 0.3825	0.1879 \pm 0.5527	0.1283 \pm 0.2364	0.3116 \pm 0.6958	94.25	0.2106 \pm 0.6129	96.26
	0.1393 \pm 0.3402	0.1842 \pm 0.5479	0.1249 \pm 0.2272	0.3023 \pm 0.6671		0.2023 \pm 0.5920	96.59

Table 5: Best performance of PhysGNN on Dataset 1 and 2.

Dataset	δy_{max} (mm)	δy_{mean} (mm)	Max. Euclidean Error _{mean} (mm)
1	24.5864	11.6229 \pm 5.7681	2.5924 \pm 1.5665
2	47.8233	16.4170 \pm 10.4650	4.1952 \pm 2.5161

Table 6: The test set statistics of Dataset 1 and 2, where y is the displacement, and Max. Euclidean Error_{mean} is computed as the average of the maximum Euclidean error observed for each data element—i.e. each FE simulation.

where $|\mathcal{V}|$ is the number of mesh nodes, $\mathbf{y} \in \mathbb{R}^{|\mathcal{V}| \times 3}$ is the displacement in the x , y , and z directions approximated by the FEM, and $\mathbf{z} \in \mathbb{R}^{|\mathcal{V}| \times 3}$ is the displacement predicted by PhysGNN. To minimize the loss value, AdamW optimizer was used with an initial learning rate of 0.005, which was reduced by a factor of 0.1 to a minimum value of 1e-8 if no improvement on the validation loss was noticed after 5 epochs.

Regularization

Early stopping was one of the regularization methods implemented by which learning stopped after no decrease in validation loss occurred after 15 epochs. Moreover, a dropout rate of 0.1 was applied to the second last layer of PhysGNN to improve generalization to unseen data.

Infrastructure Settings

The experiments in our study were carried on a Google Colab Pro server with 23GB of RAM, and one NVIDIA P-100 GPU with 16 GB of video RAM.

Results and Discussion

Performance of PhysGNN in Predicting Tissue Deformation

Table 5 is indicative of the performance of the PhysGNN configurations that resulted in the lowest validation loss on Dataset 1 and Dataset 2, illustrated in Figures 4a and 4b. According to the results, PhysGNN is capable of effectively predicting tissue deformation under prescribed loads, especially highlighted by 96% and 97% of absolute position errors being under 1mm in Datasets 1 and 2 respectively. Moreover, prediction of tissue deformation per each FE simulation on an NVIDIA P-100 GPU took 0.0043 ± 0.0005 seconds, while it took 1.8294 ± 0.0322 seconds on a dual core

Intel(R) Xeon(R) @ 2.20GHz CPU. Based on these observations and the fact that the accuracy in neurosurgery is not better than 1mm [Miller et al. 2010], PhysGNN manifests itself as a promising deep learning module for predicting tissue deformation in neurosurgical settings for providing both high accuracy and computational speed.

Comparison to Similar Studies

Comparing our results with the most recent works on predicting tissue deformation with machine learning methods, our approach compares favourably. In [Tonutti et al. 2017] the authors investigate tissue deformation of a brain tumour upon forces less than 1N to a single node on the brain surface at a time and report a mean absolute position error of $0.191 \pm 0.201\text{mm}$. While our absolute position error for Dataset 1 (where forces $\leq 1.35\text{N}$ are applied to a single node) seems to only be marginally smaller than theirs, we argue that our result is implicitly much better as our test set contains larger deformations since we consider for both the brain and tumour tissues. Similarly, our proposed method appears to be competitive with the results in [Lorente et al. 2017] where they report 100% of the Euclidean errors to be $\leq 1\text{mm}$, for a dataset with a maximum displacement of 15 mm. Lastly, Liu et al. [2020] report an average Euclidean error of 0.129mm and 0.392 mm, and an average maximum Euclidean error of 0.483mm and 1.011 mm for two different test sets that exhibit a maximum displacement of 30mm on a mesh with 1158 nodes. By referring to Tables 5 and 6, our results (achieved on a mesh with 9118 nodes) are shown to be competitive without requiring PCA to reduce the subspace dimensionality. Indeed, GNNs are inherently graph embedding models which encode graphs into a lower dimensional subspace to facilitate data manipulation for carrying out machine learning tasks on graphs. Therefore, we deem our method to not only effective for predicting tissue deformation but also a simpler approach to implement.

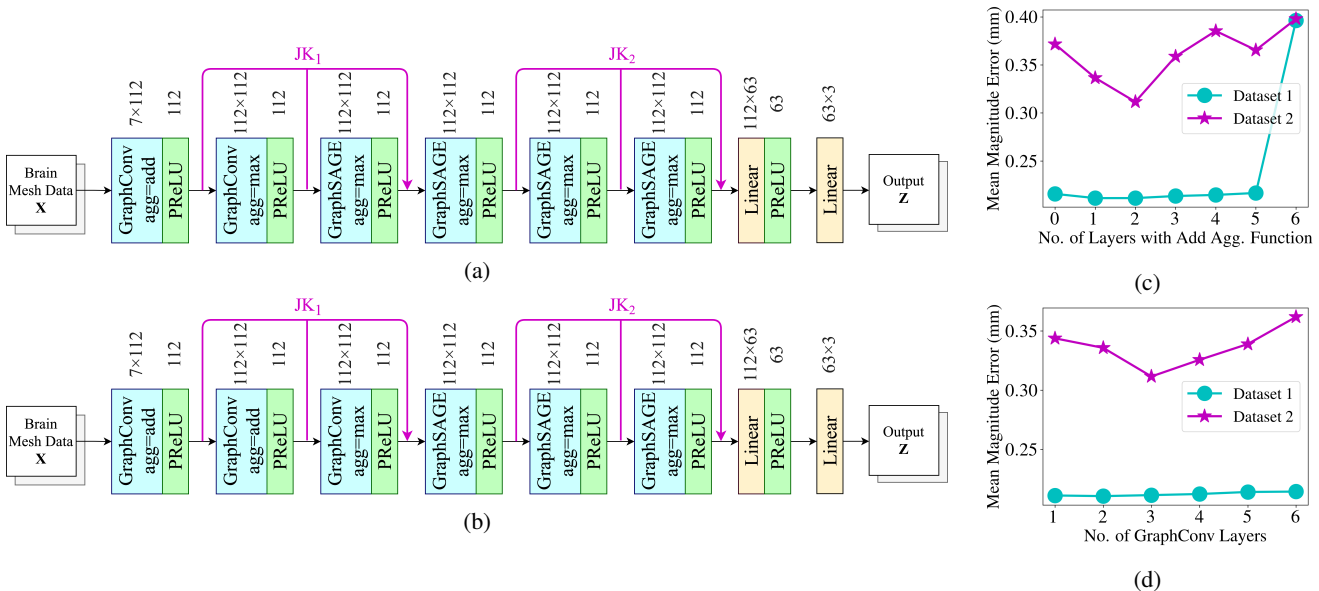


Figure 4: Best performing PhysGNN configuration on (a) Dataset 1, and (b) Dataset 2. The effect of (c) replacing maximum with the addition aggregation function in a PhysGNN model consisting of 3 GraphConv layers followed by 3 GraphSAGE layers, and (d) consecutive replacement of GraphSAGE with GraphConv layers while using the best performing aggregation function combination. Agg. stands for aggregation.

Ablation Study

In our experimental study, we found the configuration of the best performing PhysGNN to be dependent on the nature of the dataset. Initializing the PhysGNN model with 3 GraphConv layers followed by 3 GraphSAGE layers, consecutive replacement of maximum with addition aggregation function for two iterations reduced the mean validation Euclidean loss of Dataset 2 more noticeably, while such replacement for five iterations only marginally changed the performance of PhysGNN on the validation set of Dataset 1, as shown in Figure 4c. This observation is justified by realizing that nodal displacements in Dataset 1 are resulted from applying forces to only one node, contrary to nodal displacements in Dataset 2 which occur from multiple prescribed force nodes. Consequently, while using the maximum aggregation function in different GNN layers would be a more reasonable choice when training PhysGNN with Dataset 1, summing prescribed forces applied to the nodes within the same neighbourhood results in more accurate tissue displacement predictions when training PhysGNN with Dataset 2.

Similarly, replacing GraphSAGE with GraphConv layers in consecutive order while using the best performing combination of aggregation functions resulted in a more pronounced decrease in validation loss of Dataset 2, as depicted in Figure 4d, where using three GraphConv layers yielded the best performance. However, while weighting neighbouring nodes' messages with edge weights using GraphConv layers decreased loss value in both datasets for the first few iterations, it caused over-smoothing beyond a certain number. This observation sheds light on the importance of incorporating nodal distance and proper formulation of edge

weights to effectively capture tissue deformation.

Limitations and Future Directions

As mentioned by Tonutti et al. [2017], a limitation of FEM data-driven models is using the FEA results as baseline, which is dependent on the quality of MRI image segmentation, and the selected soft tissue constitutive laws that may not hold true for different patients. Moreover, tetrahedral elements are prone to undergoing volumetric locking for almost incompressible materials, such as soft tissue, and should not be used to simulate tissue deformation [Joldes et al. 2019]. To alleviate these problems, Meshless Total Lagrangian Explicit Dynamics (MTLED) algorithms are emerging as a solution to better simulate soft tissue deformation, which can also be trained with empirical results [Miller et al. 2019, Joldes et al. 2019]. As PhysGNN may also be trained with the results of Lagrangian meshless methods, the presented framework is foreseen to yield highly accurate and computationally efficient data-driven deformable volumes in the future.

Conclusion

The purpose of this work was to introduce a novel data-driven framework, PhysGNN, to combat the limitations of using the FEM for approximating tissue deformation in neurosurgical settings. Through our empirical results, we demonstrated the effectiveness of PhysGNN in accurately predicting tissue deformation. Compared to similar studies, our method is competitive with data-driven state of the art approaches for capturing tissue deformation while promising enhanced computational feasibility, especially for large and high-quality meshes.

References

Ehsan Basafa and Farzam Farahmand. Real-time simulation of the nonlinear visco-elastic deformations of soft tissues. *International journal of computer assisted radiology and surgery*, 6(3):297–307, 2011.

Steven S. Beauchemin and John L. Barron. The computation of optical flow. *ACM computing surveys (CSUR)*, 27(3):433–466, 1995.

Filipe de Avila Belbute-Peres, Thomas Economou, and Zico Kolter. Combining differentiable pde solvers and graph neural networks for fluid flow prediction. In *International Conference on Machine Learning*, pages 2402–2411. PMLR, 2020.

Chaim Broit. Optimal registration of deformed images. 1981.

Kup-Sze Choi, Hanqiu Sun, and Pheng-Ann Heng. An efficient and scalable deformable model for virtual reality-based medical applications. *Artificial intelligence in medicine*, 32(1):51–69, 2004.

Kevin Cleary and Terry M Peters. Image-guided interventions: technology review and clinical applications. *Annual review of biomedical engineering*, 12:119–142, 2010.

William R Crum, Thomas Hartkens, and DLG Hill. Non-rigid image registration: theory and practice. *The British journal of radiology*, 77(suppl_2):S140–S153, 2004.

Suvranu De, Dhannanjay Deo, Ganesh Sankaranarayanan, and Venkata S Arikatla. A physics-driven neural networks-based simulation system (phynness) for multimodal interactive virtual environments involving nonlinear deformable objects. *Presence: Teleoperators and Virtual Environments*, 20(4):289–308, 2011.

Matthieu Ferrant, Arya Nabavi, Benoit Macq, Peter M Black, Ferenc A Jolesz, Ron Kikinis, and Simon K Warfield. Serial registration of intraoperative mr images of the brain. *Medical image analysis*, 6(4):337–359, 2002.

Liu Shi Gan, Kourosh Zareinia, Sanju Lama, Yaser Madadihi, Fang Wei Yang, and Garnette R Sutherland. Quantification of forces during a neurosurgical procedure: A pilot study. *World neurosurgery*, 84(2):537–548, 2015.

Justin Gilmer, Samuel S Schoenholz, Patrick F Riley, Oriol Vinyals, and George E Dahl. Neural message passing for quantum chemistry. In *International conference on machine learning*, pages 1263–1272. PMLR, 2017.

Alexander Hagemann, Karl Rohr, H Siegfried Stiehl, Uwe Spetzger, and Joachim M Gilsbach. Biomechanical modeling of the human head for physically based, nonrigid image registration. *IEEE transactions on medical imaging*, 18(10):875–884, 1999.

Will Hamilton, Zhitao Ying, and Jure Leskovec. Inductive representation learning on large graphs. In *Advances in neural information processing systems*, pages 1024–1034, 2017a.

William L Hamilton. Graph representation learning. *Synthesis Lectures on Artificial Intelligence and Machine Learning*, 14(3):1–159, 2020.

William L Hamilton, Rex Ying, and Jure Leskovec. Representation learning on graphs: Methods and applications. *arXiv preprint arXiv:1709.05584*, 2017b.

Nobuhiko Hata, Arya Nabavi, William M Wells III, Simon K Warfield, Ron Kikinis, Peter McL Black, and Ferenc A Jolesz. Three-dimensional optical flow method for measurement of volumetric brain deformation from intraoperative mr images. *Journal of Computer Assisted Tomography*, 24(4):531–538, 2000.

Daniel Høyer Iversen, Wolfgang Wein, Frank Lindseth, Geirmund Unsgård, and Ingerid Reinertsen. Automatic intraoperative correction of brain shift for accurate neuronavigation. *World neurosurgery*, 120:e1071–e1078, 2018.

Songbai Ji, Xiaoyao Fan, David W Roberts, Alex Hartov, and Keith D Paulsen. Cortical surface shift estimation using stereovision and optical flow motion tracking via projection image registration. *Medical image analysis*, 18(7):1169–1183, 2014.

Grand Joldes, George Bourantas, Benjamin Zwick, Habib Chowdhury, Adam Wittek, Sudip Agrawal, Konstantinos Mountris, Damon Hyde, Simon K Warfield, and Karol Miller. Suite of meshless algorithms for accurate computation of soft tissue deformation for surgical simulation. *Medical image analysis*, 56:152–171, 2019.

Grand Roman Joldes, Adam Wittek, and Karol Miller. Suite of finite element algorithms for accurate computation of soft tissue deformation for surgical simulation. *Medical image analysis*, 13(6):912–919, 2009.

Grand Roman Joldes, Adam Wittek, and Karol Miller. Real-time nonlinear finite element computations on gpu-application to neurosurgical simulation. *Computer methods in applied mechanics and engineering*, 199(49–52):3305–3314, 2010.

Thomas N Kipf and Max Welling. Semi-supervised classification with graph convolutional networks. *arXiv preprint arXiv:1609.02907*, 2016.

Ping Li, Weiwei Wang, Zhijian Song, Yong An, and Chenxi Zhang. A framework for correcting brain retraction based on an extended finite element method using a laser range scanner. *International journal of computer assisted radiology and surgery*, 9(4):669–681, 2014.

Haolin Liu, Ye Han, Daniel Emerson, Houriyeh Majditehran, Qi Wang, Yoed Rabin, and Levent Burak Kara. Real-time prediction of soft tissue deformations using data-driven nonlinear presurgical simulations. *arXiv preprint arXiv:2010.13823*, 2020.

Delia Lorente, Francisco Martínez-Martínez, María José Rupérez, MA Lago, Marcelino Martínez-Sober, Pablo Escandell-Montero, José María Martínez-Martínez, Sandra Martínez-Sanchis, Antonio J Serrano-López, C Monserat, et al. A framework for modelling the biomechanical behaviour of the human liver during breathing in real time using machine learning. *Expert Systems with Applications*, 71:342–357, 2017.

Steve A Maas, Benjamin J Ellis, Gerard A Ateshian, and Jeffrey A Weiss. Febio: finite elements for biomechanics. *Journal of biomechanical engineering*, 134(1), 2012.

Subha Madhavan, Jean-Claude Zenklusen, Yuri Kotliarov, Himanso Sahni, Howard A Fine, and Kenneth Buetow. Rembrandt: helping personalized medicine become a reality through integrative translational research. *Molecular cancer research*, 7(2):157–167, 2009.

Hani R Malone, Omar N Syed, Michael S Downes, Anthony L D’Ambrosio, Donald O Quest, and Michael G Kaiser. Simulation in neurosurgery: a review of computer-based simulation environments and their surgical applications. *Neurosurgery*, 67(4):1105–1116, 2010.

Karol Miller, Grand Joldes, Dane Lance, and Adam Wittek. Total lagrangian explicit dynamics finite element algorithm for computing soft tissue deformation. *Communications in numerical methods in engineering*, 23(2):121–134, 2007.

Karol Miller, Adam Wittek, and Grand Joldes. Biomechanics of the brain for computer-integrated surgery. *ACTA of Bioengineering and Biomechanics*, 12(2):25–37, 2010.

Karol Miller, Grand R Joldes, George Bourantas, Simon K Warfield, Damon E Hyde, Ron Kikinis, and Adam Wittek. Biomechanical modeling and computer simulation of the brain during neurosurgery. *International journal for numerical methods in biomedical engineering*, 35(10):e3250, 2019.

Kevin M Moerman. Gibbon: the geometry and image-based bioengineering add-on. *Journal of Open Source Software*, 3(22):506, 2018.

Christopher Morris, Martin Ritzert, Matthias Fey, William L Hamilton, Jan Eric Lenssen, Gaurav Rattan, and Martin Grohe. Weisfeiler and leman go neural: Higher-order graph neural networks. In *Proceedings of the AAAI Conference on Artificial Intelligence*, volume 33, pages 4602–4609, 2019.

Arya Nabavi, Peter McL. Black, David T Gering, Carl-Fredrik Westin, Vivek Mehta, Richard S Pergolizzi Jr, Mathieu Ferrant, Simon K Warfield, Nobuhiko Hata, Richard B Schwartz, et al. Serial intraoperative magnetic resonance imaging of brain shift. *Neurosurgery*, 48(4):787–798, 2001.

Tobias Pfaff, Meire Fortunato, Alvaro Sanchez-Gonzalez, and Peter Battaglia. Learning mesh-based simulation with graph networks. In *International Conference on Learning Representations*, 2020.

Micha Pfeiffer, Carina Riediger, Jürgen Weitz, and Stefanie Speidel. Learning soft tissue behavior of organs for surgical navigation with convolutional neural networks. *International journal of computer assisted radiology and surgery*, 14(7):1147–1155, 2019.

Petter Risholm, Alexandra J Golby, and William Wells. Multimodal image registration for preoperative planning and image-guided neurosurgical procedures. *Neurosurgery Clinics*, 22(2):197–206, 2011.

David W Roberts, Alexander Hartov, Francis E Kennedy, Michael I Miga, and Keith D Paulsen. Intraoperative brain shift and deformation: a quantitative analysis of cortical displacement in 28 cases. *Neurosurgery*, 43(4):749–758, 1998.

Alvaro Sanchez-Gonzalez, Nicolas Heess, Jost Tobias Springenberg, Josh Merel, Martin Riedmiller, Raia Hadsell, and Peter Battaglia. Graph networks as learnable physics engines for inference and control. In *International Conference on Machine Learning*, pages 4470–4479. PMLR, 2018.

Alvaro Sanchez-Gonzalez, Jonathan Godwin, Tobias Pfaff, Rex Ying, Jure Leskovec, and Peter Battaglia. Learning to simulate complex physics with graph networks. In *International Conference on Machine Learning*, pages 8459–8468. PMLR, 2020.

Franco Scarselli, Marco Gori, Ah Chung Tsoi, Markus Hagenbuchner, and Gabriele Monfardini. The graph neural network model. *IEEE Transactions on Neural Networks*, 20(1):61–80, 2008.

Hang Si. Tetgen, a delaunay-based quality tetrahedral mesh generator. *ACM Transactions on Mathematical Software (TOMS)*, 41(2):1–36, 2015.

Hai Sun, Francis E Kennedy, Erik J Carlson, Alex Harrov, David W Roberts, and Keith D Paulsen. Modeling of brain tissue retraction using intraoperative data. In *International Conference on Medical Image Computing and Computer-Assisted Intervention*, pages 225–233. Springer, 2004.

Michele Tonutti, Gauthier Gras, and Guang-Zhong Yang. A machine learning approach for real-time modelling of tissue deformation in image-guided neurosurgery. *Artificial intelligence in medicine*, 80:39–47, 2017.

Zhigang Tu, Wei Xie, Dejun Zhang, Ronald Poppe, Remco C Veltkamp, Baoxin Li, and Junsong Yuan. A survey of variational and cnn-based optical flow techniques. *Signal Processing: Image Communication*, 72:9–24, 2019.

Lara M Vigneron, Jacques G Verly, and Simon K Warfield. Modelling surgical cuts, retractions, and resections via extended finite element method. In *International Conference on Medical Image Computing and Computer-Assisted Intervention*, pages 311–318. Springer, 2004.

Lara M Vigneron, Romain C Boman, Jean-Philippe Ponthot, Pierre A Robe, Simon K Warfield, and Jacques G Verly. Enhanced fem-based modeling of brain shift deformation in image-guided neurosurgery. *Journal of Computational and Applied Mathematics*, 234(7):2046–2053, 2010.

Simon K Warfield, Matthieu Ferrant, Xavier Gallez, Arya Nabavi, Ferenc A Jolesz, and Ron Kikinis. Real-time biomechanical simulation of volumetric brain deformation for image guided neurosurgery. In *SC’00: Proceedings of the 2000 ACM/IEEE Conference on Supercomputing*, pages 23–23. IEEE, 2000.

Adam Wittek, Trent Hawkins, and Karol Miller. On the unimportance of constitutive models in computing brain deformation for image-guided surgery. *Biomechanics and modeling in mechanobiology*, 8(1):77–84, 2009.

Adam Wittek, Grand Joldes, Mathieu Couton, Simon K Warfield, and Karol Miller. Patient-specific non-linear finite element modelling for predicting soft organ deformation in real-time; application to non-rigid neuroimage registration. *Progress in biophysics and molecular biology*, 103(2-3):292–303, 2010.

Keyulu Xu, Chengtao Li, Yonglong Tian, Tomohiro Sonobe, Ken-ichi Kawarabayashi, and Stefanie Jegelka. Representation learning on graphs with jumping knowledge networks. In *International Conference on Machine Learning*, pages 5453–5462. PMLR, 2018.

Jinao Zhang, Yongmin Zhong, and Chengfan Gu. Deformable models for surgical simulation: a survey. *IEEE reviews in biomedical engineering*, 11:143–164, 2017.

Jinao Zhang, Yongmin Zhong, and Chengfan Gu. Neural network modelling of soft tissue deformation for surgical simulation. *Artificial intelligence in medicine*, 97:61–70, 2019.

Yongmin Zhong, Bijan Shirinzadeh, Gürsel Alici, and Julian Smith. A cellular neural network methodology for deformable object simulation. *IEEE Transactions on Information technology in Biomedicine*, 10(4):749–762, 2006.